

## RAREFACTION EFFECTS ON GALILEO PROBE AERODYNAMICS

James N. Moss, Gerald J. LeBeau, Robert C. Blanchard, Joseph M. Price  
(Aerothermodynamics Branch, NASA Langley Research Center, Hampton, Virginia 23681-0001, USA)

**ABSTRACT:** Solutions of aerodynamic characteristics are presented for the Galileo Probe entering Jupiter's hydrogen-helium atmosphere at a nominal relative velocity of 47.4 km/s. Focus is on predicting the aerodynamic drag coefficient during the transitional flow regime using the direct simulation Monte Carlo (DSMC) method. Accuracy of the probe's drag coefficient directly impacts the inferred atmospheric properties that are being extracted from the deceleration measurements made by onboard accelerometers as part of the Atmospheric Structure Experiment. The range of rarefaction considered in the present study extends from the free molecular limit to continuum conditions. Comparisons made with previous calculations and experimental measurements show the present results for drag to merge well with Navier-Stokes and experimental results for the least rarefied conditions considered.

### 1 INTRODUCTION

Project Galileo is a NASA spacecraft mission to Jupiter, designed to study the planet's atmosphere, satellites, and surrounding magnetosphere. The mission consisted of both an orbiter and a probe. A significant mission milestone occurred December 7, 1995, when the orbiter achieved an orbit about Jupiter and the Galileo Probe made a successful entry into Jupiter's hydrogen-helium atmosphere at a relative velocity of approximately 47.4 km/s. The Atmospheric Structure Experiment<sup>1</sup>, one of six experiments flown on the probe, measured deceleration from the high-altitude entry phase through the final descent phase. At subsonic conditions a descent module, which contained the instrument package, was extracted from the probe and continued to descend on a parachute until the mission was terminated due to high pressure/temperature conditions. Prior to extraction of the descent module, this experiment is being used to deduce atmospheric density, pressure, and temperature from probe deceleration measurements. The atmospheric properties can be inferred during the rarefied portion of entry provided information is known concerning the probe drag coefficient and velocity.

Accuracy of the Atmospheric Structure Experiment depends directly on the accuracy of the probe drag coefficient. Consequently, the focus of the present study is the simulation of the aerodynamics from altitudes exceeding the threshold of the measurements to continuum conditions (spanning more than 1000 km according to recently inferred<sup>1</sup> atmospheric data).

The first calculations addressing the transitional flow regime for the Galileo Probe entry were those of Ref. 2 where direct simulation Monte Carlo (DSMC) solutions were presented for freestream Reynolds number based on probe diameter of  $\leq 1,000$ . In the present study, the DSMC calculations are extended to higher Reynolds number conditions ( $\leq 79,000$ ) to cover the entire transitional flow regime and to address questions raised by ballistic range tests<sup>3</sup> conducted at NASA Ames. As discussed in Ref. 4 these tests showed a minimum in the drag coefficient at a Reynolds number of 10,000. The present calculations show no evidence of such a minimum. DSMC results from both axisymmetric and three-dimensional solvers are presented.

### 2 PROBLEM DEFINITION

#### 2.1 Computational Methods

The 2D/axisymmetric DSMC code of Bird<sup>5</sup> was used for calculating the results included in Table 1. These calculations included the Galileo Probe forebody (Fig. 1) and cylindrical extension, but not the afterbody. The drag contribution of the Galileo Probe afterbody is negligible for hypersonic flow as demonstrated herein and in Ref. 4. The 3D

DSMC calculations for both forebody and afterbody were made by the second author using a relatively new algorithm named DAC (DSMC Analysis Code). The DAC code utilizes an unstructured triangular grid for defining the surface with the volume grid consisting of a Cartesian network of cells where each level-1 Cartesian cell can have additional Cartesian refinement. This ability to refine the flowfield grid locally allows DAC to meet the spatial resolution requirement of the DSMC method without excessive global refinement. More details concerning the DAC features and capabilities are included in Ref. 6.

The 3D calculations using the DAC code were made only for the more rarefied portion of the entry ( $Kn_{\infty} \geq 0.02$ ). For the axisymmetric probe, only half of the flowfield is simulated utilizing a plane of symmetry. The number of simulated molecules used in these simulations ranged from about 100,000 to  $5.2 \times 10^6$  and the corresponding number of cells from 10,000 to 600,000.

The axisymmetric computations made with the G2 code utilized a body fitted grid. The computational domain included the forebody and the 41.15 mm cylindrical extension (Fig. 1), but not the afterbody. Fifty-one computational cells were used along the body surface for all calculations. The number of computational cells ranged from 2,601 to 12,750 and the number of simulated molecules ranged from about 40,000 to 220,000. Each computational cell was also subdivided into four subcells which promotes collisions between near neighbors.

Molecular collisions are simulated using the variable hard sphere (VHS)<sup>7</sup> molecular model. Parameters used to define the VHS model were a reference temperature of 273 K, reference diameters of  $2.92 \times 10^{-10}$  m and  $2.33 \times 10^{-10}$  m for hydrogen and helium, respectively, and the temperature exponent coefficient of viscosity was set to 0.67. Energy exchange between kinetic and internal modes was controlled by the Larsen-Borgnakke statistical model. Unless noted otherwise, the calculations were performed using a nonreacting gas model with two chemical species (89% H<sub>2</sub> and 11% He by volume) while considering energy exchange between translational, rotational, and vibrational modes. For hydrogen, a rotational relaxation collision number of 5 and a vibrational relaxation collision number of 50 (vibrational effects not included in DAC calculations) were used with a characteristic vibrational temperature of 6100 K.

For the gas surface interaction, the gas molecules were assumed to be reflected diffusively with full thermal accommodation at a specified surface temperature (Table 1).

## 2.2 Galileo Probe

The Galileo Probe configuration and dimensions are given in Fig. 1. Thermal protection materials formed the outer surface of the probe with carbon phenolic ablation material along the forebody and phenolic-nylon material along the afterbody. The mass of the probe at entry was 338.93 kg. The onset of ablation occurred near 215 km.

## 2.3 Freestream Conditions

The freestream conditions listed in Table 1 were generated from a preflight trajectory analysis using an Orton<sup>8</sup> model for the atmosphere. Zero altitude is a location within Jupiter's atmosphere where the pressure equals 1.0 bar. The time for the Galileo Probe to traverse the range of conditions considered was 85 s.

Recent results<sup>1</sup> based on the Galileo probe measurements indicate that the density data essentially coincide with the Orton model below 290 km but depart from it at higher altitudes; at 1000 km, densities were 100 times the model density. Consequently, the results presented for the probe drag should be viewed in terms of variation with density or Knudsen number rather than altitudes. Also, since the lowest density condition considered was  $4.454 \times 10^{-12}$  kg/m<sup>3</sup>, the upper atmosphere altitude based on the new data<sup>1</sup> would be in excess of 1200 km rather than 833 km.

# 3 RESULTS

## 3.1 Present Computations

Included in Table 1 are values for drag-coefficient, acceleration, and stagnation-point heating rate obtained with the G2 code. The heating results will not be emphasized since the

values are much too high at the lower altitude conditions due to lack of accounting for chemical reactions and mass injection from the thermal protection materials.

Drag results from both axisymmetric (G2) and three-dimensional (DAC) DSMC codes are presented in Fig. 2. Shown is the drag coefficient as a function of freestream Knudsen number (characteristic length = 1.2649 m). Evident is the significant increase in the magnitude of the drag coefficient as the flow rarefaction increases from continuum to free molecular conditions, approaching the free molecular value of 2.04. Also shown is the pressure component of the drag coefficient which varies only 6 percent over the transitional flow regime. For the range of conditions considered, the frictional drag component increases from 5.8 percent of the total drag at  $Kn_\infty = 0.00086$  to 47.4 percent at a  $Kn_\infty = 1,910$ .

As shown in Fig. 2, the results from the two DSMC solutions are in excellent agreement for the total drag as well as the pressure and frictional components. Also, the effect of angle of attack was investigated for the  $Kn_\infty = 0.22$  condition. For  $\alpha = 5^\circ$ , the DAC solution gives axial and normal forces coefficients of  $C_A = 1.731$  and  $C_N = 0.140$ . For this transitional flow condition, a 5-deg angle of incidence produces a very small change in the axial coefficient compared to the zero incident case (0.79 percent reduction).

Preliminary results from the Galileo Probe accelerometer measurements show that the angle of incidence was 5.5 degs or less during the hypersonic portion of the deceleration measurements. Furthermore, the maximum angle of incidence occurs at free molecular conditions and in general decreases with decreasing altitude. Consequently, the zero incidence results for the axial or drag coefficient are a good approximation for the range of entry conditions considered in the present study.

Selected distributions of surface pressure and skin friction are presented in Figs. 3 and 4, respectively, demonstrating their sensitivity to rarefaction effects. The results are presented as a function of wetted distance,  $s$ , along the body surface. The increase in the pressure coefficient on the spherical nose section with increasing rarefaction is qualitatively correct. On the conical frustum, the pressure coefficient distribution is also seen to be influenced by rarefaction. For the smallest Knudsen number case considered, there is a substantial over expansion followed by recompression that influences the entire conical portion of the forebody. This process diminishes with increasing rarefaction. The pressure coefficient along the conical forebody is a maximum for a Knudsen number of 0.22 (Fig. 3) and exceeds the free molecular value for this set of flow and surface conditions by about 5 percent, hence, the maximum pressure contribution to the drag coefficient as observed in Fig. 2.

The skin friction coefficient increases substantially with rarefaction (Fig. 4) such that the drag due to friction comprises about 48 percent of the total drag in the free molecular limit. Maximum values of the skin friction coefficient occur either on the spherical nose section or preceding the expansion of the flow about the sharp outer corner.

Calculations were made to investigate the effects that chemical reactions might have on the calculated drag. Three dissociation reactions for  $H_2$  colliding with  $H_2$ ,  $H$ , and  $He$  were implemented using ad hoc rate coefficients and arbitrarily adjusting the magnitude of the pre-exponential constants in the modified Arrhenius equation. Calculations made for the  $Kn_\infty = 0.0078$  case showed the effects of the finite chemical reactions to be negligible (fraction of a percent) on the drag while producing significant levels of dissociation and reduction in surface heating.

### 3.2 Comparisons with Computations and Experiments

The baseline drag coefficient data currently utilized for the Jupiter Atmospheric Structure experiment is based on a composite of computational and experimental results (see Fig. 4 of Ref. 4). Figure 5 presents the baseline data and the current G2 results for the freestream conditions considered in the current study. The shape of the baseline data curve is based primarily on the DSMC analysis of Ref. 2 for the higher Knudsen number ( $\geq 0.07$ ) flow conditions and the Ames ballistic range results for Knudsen numbers  $\leq 0.01$ . The baseline data differs by no more than 6 percent from the current results in the more rarefied portion of the transitional regime but by as much as 24 percent for the smaller Knudsen number conditions.

A more detailed breakout of the baseline results is given in Fig. 6. Here the present results, as a function of freestream Reynolds number, are compared with the DSMC results of Ref. 2, the ballistic range data presented in Ref. 4 and recent Navier Stokes results from Ref. 4. The Navier-Stokes solutions<sup>4</sup> included the effects of chemical reactions for a gas composition of 0.89 H<sub>2</sub> and 0.11 He by volume. No-slip and zero mass injection boundary conditions were utilized. Issues and concerns related to the ballistic range tests for low Reynolds number conditions are discussed in Refs. 2, 3, and 4.

The present results are shown to blend in well with both the Navier-Stokes and the ballistic range data for Reynolds numbers approaching 10<sup>5</sup>. Neither the current nor the Navier Stokes results agree with the experimental results for the lower Reynolds number conditions of the ballistic tests; the experimental results produce lower values for the drag coefficient and a minimum at Re<sub>∞</sub> = 10,000. The current DSMC computations and the Navier Stokes results<sup>4</sup> provide an improved definition of the drag coefficient data to be used in the ongoing Jupiter atmospheric definition.

#### 4 CONCLUDING REMARKS

Results of calculations using the DSMC method are presented for the Galileo Probe entering Jupiter's hydrogen-helium atmosphere. Drag coefficient results critical to the accuracy of the Atmospheric Structure Experiment flown on Galileo are presented for the transitional flow regime. This flow regime covers more than 1000 km of Jupiter's atmosphere based on recently revised state properties of Jupiter's atmosphere. Solutions obtained using two DSMC codes, an axisymmetric code (G2) with an extensive history of testing/validation and a relatively new 3-D code (DAC), are shown to agree extremely well in predicting the probe aerodynamics. Also, the current drag results are shown to merge well with Navier Stokes and experimental results for Knudsen numbers ≤ 0.001. The present findings do not support the ballistic range experiments for Reynolds numbers <10<sup>5</sup>.

#### REFERENCES

- [1] Seiff, A., Kirk, D. B., Knight, T. C. D., Mihalov, J. D., Blanchard, R. C., Young, R. E., Schubert, G., Von Zahn, U., Lehmachet, G., Milos, F. S., and Wang, J. Structure of the Atmosphere of Jupiter: Galileo Probe Measurements. *Science*, vol. 272, 10 May 1996, pp. 884-885.
- [2] Haas, B. L. and Milos, F. S. Simulated Rarefied Entry of the Galileo Probe into the Atmosphere of Jupiter. AIAA Paper 94-2043.
- [3] Intrieri, P. F. and Kirk, D. B. High-Speed Aerodynamics of Several Blunt-Cone Configurations. *Journal of Spacecraft*, vol. 24, no. 2, 1987, pp. 127-132.
- [4] Seiff, A., Venkatapathy, E., Haas, B., and Intrieri, P. Galileo Probe Aerodynamics. AIAA Paper 96-2451.
- [5] Bird, G. A. *The G2/A3 Program Users Manual*. G.A.B. Consulting Pty Ltd, Killara, N.S.W., Australia, March 1992.
- [6] Wilmoth, R. G., LeBeau, G. J., and Carlson, A. B. DSMC Grid Methodologies for Computing Low-Density Hypersonic Flows about Reusable Launch Vehicles. AIAA Paper 96-1812.
- [7] Bird, G. A. *Molecular Gas Dynamics and the Direct Simulation of Gas Flows*. Clarendon Press, Oxford, 1994.
- [8] Orton, G. S. Jet Propulsion Laboratory Report 1625-125, NASA, 1981.

Table 1. Flight Conditions<sup>a</sup> and Results of DSMC Simulations for Galileo Probe

Altitude, km	$V_{\infty}$ , km/s	$n_{\infty}$ , $m^{-3}$	$T_{\infty}$ , K	$T_w$ , K	$Kn_{\infty}$	$Re_{\infty}$	$C_D$	Acceleration <sup>b</sup> , g	Stagnation Heating <sup>c</sup> , MW/m <sup>2</sup>
833.2	47.220	$1.199 \times 10^{15}$	589.6	300	$1.91 \times 10^3$	$1.93 \times 10^{-2}$	2.038	$3.83 \times 10^{-4}$	$2.25 \times 10^{-4}$
753.3	47.258	$3.932 \times 10^{15}$	459.4	300	$5.57 \times 10^2$	$7.50 \times 10^{-2}$	2.036	$1.26 \times 10^{-3}$	$7.60 \times 10^{-4}$
675.8	47.295	$1.432 \times 10^{16}$	397.0	300	$1.49 \times 10^2$	$3.01 \times 10^{-1}$	2.027	$4.56 \times 10^{-3}$	$2.73 \times 10^{-3}$
600.7	47.332	$5.435 \times 10^{16}$	358.7	350	$3.86 \times 10^1$	$1.23 \times 10^0$	2.012	$1.72 \times 10^{-4}$	$1.07 \times 10^{-2}$
528.0	47.367	$2.341 \times 10^{17}$	317.1	380	$8.78 \times 10^0$	$5.74 \times 10^0$	1.952	$7.20 \times 10^{-4}$	$4.37 \times 10^{-2}$
492.5	47.384	$5.187 \times 10^{17}$	294.6	395	$3.91 \times 10^0$	$1.34 \times 10^1$	1.914	$1.57 \times 10^{-3}$	$1.00 \times 10^{-1}$
457.6	47.401	$1.218 \times 10^{18}$	270.7	410	$1.64 \times 10^0$	$3.32 \times 10^1$	1.866	$3.59 \times 10^{-3}$	$2.28 \times 10^{-1}$
423.4	47.418	$3.084 \times 10^{18}$	244.9	620	$6.38 \times 10^{-1}$	$9.00 \times 10^1$	1.826	$8.89 \times 10^{-3}$	$5.64 \times 10^{-1}$
389.7	47.433	$8.677 \times 10^{18}$	216.5	800	$2.22 \times 10^{-1}$	$2.75 \times 10^2$	1.735	$2.38 \times 10^{-2}$	$1.49 \times 10^0$
356.7	47.447	$2.623 \times 10^{19}$	196.1	1050	$7.22 \times 10^{-2}$	$8.88 \times 10^2$	1.566	$6.50 \times 10^{-2}$	$4.02 \times 10^0$
324.2	47.457	$7.982 \times 10^{19}$	187.4	1500	$2.36 \times 10^{-2}$	$2.79 \times 10^3$	1.370	$1.73 \times 10^{-1}$	$9.82 \times 10^0$
292.4	47.460	$2.389 \times 10^{20}$	183.5	2100	$7.80 \times 10^{-3}$	$8.46 \times 10^3$	1.236	$4.67 \times 10^{-1}$	$2.01 \times 10^1$
261.1	47.444	$7.178 \times 10^{20}$	179.6	2700	$2.60 \times 10^{-3}$	$2.58 \times 10^4$	1.152	$1.31 \times 10^0$	$3.36 \times 10^1$
230.6	47.359	$2.161 \times 10^{21}$	175.7	3200	$8.60 \times 10^{-4}$	$7.87 \times 10^4$	1.100	$3.75 \times 10^0$	$5.80 \times 10^1$

<sup>a</sup>Freestream mole fractions are  $X_{H_2} = 0.89$  and  $X_{He} = 0.11$ ; molecular weight = 2.238; and diffuse surface with full thermal accommodation.

<sup>b</sup>Mass of probe = 338.93 kg and base area =  $1.25673 \text{ m}^2$ .

<sup>c</sup>Values are too high at lower altitudes since chemical reactions and surface blowing was not accounted for.

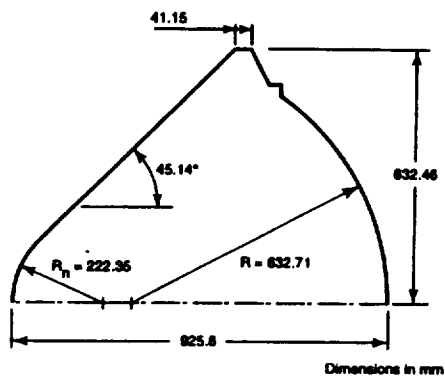


Fig 1. Galileo Probe configuration.

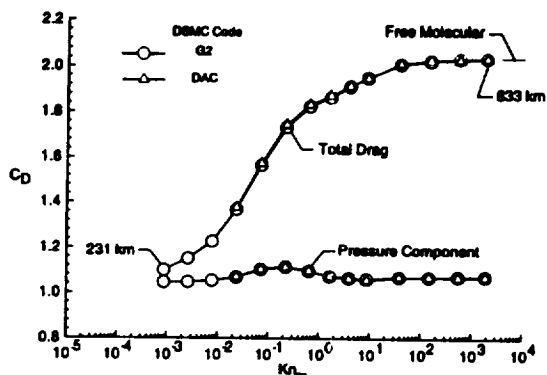


Fig 2. Calculated drag coefficients for Galileo Probe.

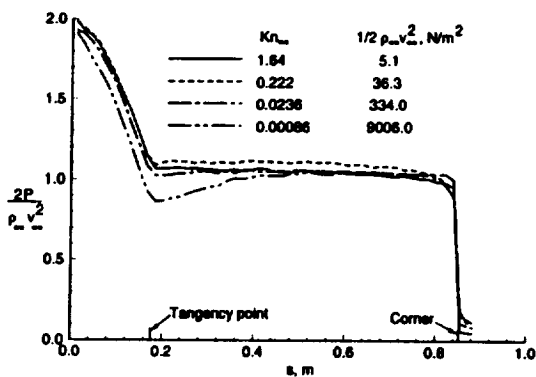


Fig 3. Effect of rarefaction on surface pressure.

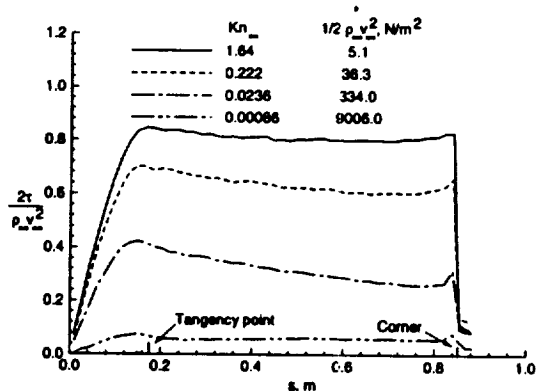


Fig 4. Effect of rarefaction on skin friction.

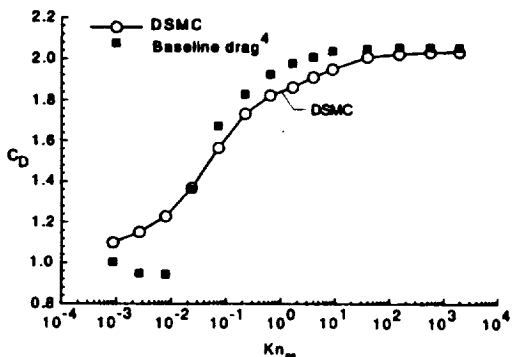


Fig 5. Baseline and current results for drag.

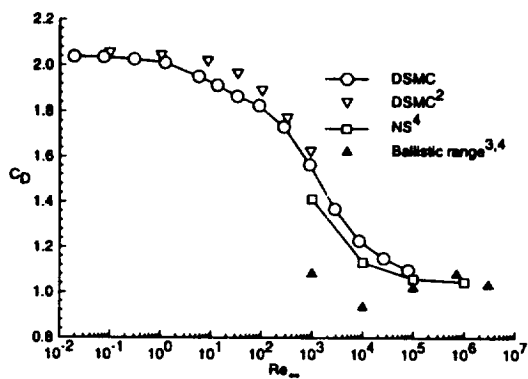


Fig 6. Computational and experimental drag results for Galileo Probe.